Acta Phys. Hung. B 20/1 (2004) 000–000

QUANTUM ELECTRONICS

Experimental Tests of Energy and Time Entanglement

Jan Soubusta[1,2,a], Jan Peřina Jr.[1,2], Ondřej Haderka[1,2], Martin Hendrych[1,2], and Miloslav Dušek[1]

[1] Department of Optics, Palacký University, 17. listopadu 50, 772 00 Olomouc, Czech Republic

[2] Joint Laboratory of Optics UP and Institute of Physics of AS CR, 17. listopadu 50A, 772 00 Olomouc, Czech Republic

Received 1 January 2004

Abstract. Entangled two-photon states are often generated in the process of spontaneous parametric down-conversion. The two photons comprising one pair are tightly correlated in energy and time. The width of these correlations are investigated in interferometric experiments. Unbalanced Mach-Zehnder interferometer in the route of one photon together with a narrow frequency filter in the route of the other one is used to evaluate the width of the energy correlations. Hong-Ou-Mandel interferometer serves for measurement of the time correlations with the same two-photon source. The measurement results approve the theoretical relation between the time and spectral (energetic) correlations expected for given entangled states. Both the strong energy correlations and narrow time correlations of the detection instants may be exhibited together only by an entangled state.

Keywords: Down-conversion, interference
PACS: 42.50.-p, 42.65.Lm

1. Introduction

Spontaneous parametric down-conversion (SPDC) often serves as a source of entangled pairs of photons. The fact, that the two photons comprising one pair are tightly correlated in energy and time, is used in many experimental applications. Different properties of SPDC were studied both theoretically and experimentally[1–3].

In this paper we study the correlations of energies of the two photons from one pair. We let the idler proton to propagate through a Mach-Zehnder (MZ) interferometer [4–11]. Scanning one arm of the MZ interferometer we measure the coherence length of the idler photons. Then we place a narrow frequency filter in the

1589-9535/04/ $ 20.00

signal photon path and observe a substantial prolongation of the coherence length behind the MZ interferometer in a coincidence-count measurement. In Section 2, the measured energy correlations are compared with the developed theoretical model. In Section 3 the time correlations are investigated measuring the Hong-Ou-Mandel interference dip with the same source and the agreement with the theory is verified [12].

2. Energy correlations

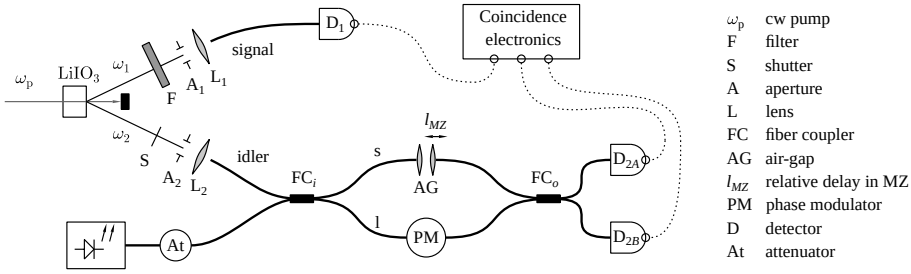

Fig. 1. Experimental setup for the measurement of energy correlations.

The experimental setup for the measurement of the energy correlations is schematically drawn in Fig. 1. The entangled two-photon state at the output plane of the nonlinear crystal is

$$|\psi^{(1)}\rangle = C_\psi \int d\omega_1 \int d\omega_2 \Phi(\omega_1, \omega_2) \hat{a}_1^\dagger(\omega_1) \hat{a}_2^\dagger(\omega_2) |\mathrm{vac}\rangle. \tag{1}$$

The symbol $\hat{a}_1^\dagger(\omega_1)$ stands for the creation operator of a photon with frequency ω_1 in the signal field and analogically the symbol $\hat{a}_2^\dagger(\omega_2)$ for the idler photon. The phase-matching function $\Phi(\omega_1, \omega_2)$ describes correlations between modes in the signal and idler fields. The normalized coincidence-count rate measured between detectors D_1 and D_{2A}, or between D_1 and D_{2B} reads

$$R_n(\Delta t) = 1 \pm \rho(\Delta t), \tag{2}$$

where ρ is an interference term, and Δt is the propagation time difference in the two arms of the MZ interferometer.

2.1. Setup with a gaussian filter

It should be stressed out, that the geometric filtering due to the apertures selects a narrow spectrum, and it can be modelled by a Gaussian curve. If we place a narrow band interference filter in the signal photon path an even narrower spectrum is

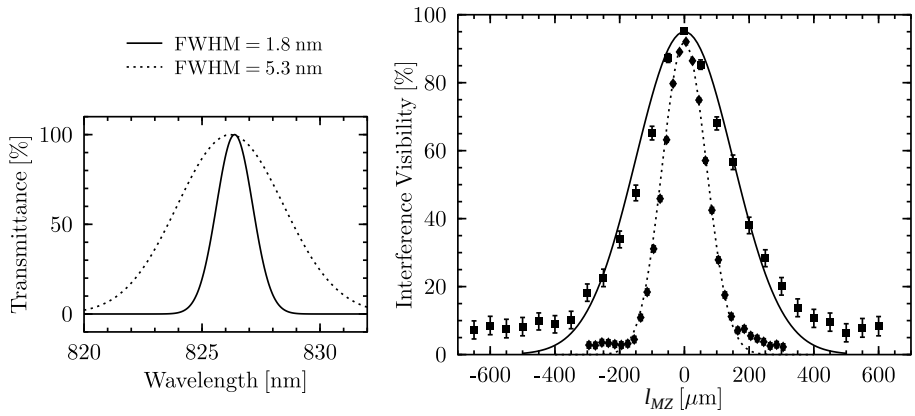

Fig. 2. Right panel: coincidence-count interference visibility as a function of the relative delay l_{MZ}: without any filter (diamonds, dotted line), with the narrow band interference filter (squares, solid line). Left panel: corresponding transmittance spectra.

selected. This spectrum can be modelled by a Gaussian curve too. The intensity spectrum reads

$$T_{Gj}(\omega_j) = \exp\left[-\frac{(\omega_j - \omega_j^0)^2}{\sigma_j^2}\right], \quad j = 1 \text{ (signal)}, 2 \text{ (idler)}. \tag{3}$$

Given the parameter σ, FWHM $= 2\sqrt{\ln 2}\sigma$. The interference term is described by the formula

$$\rho(\Delta t) = \frac{2}{C_G}\mathrm{Re}\left\{T_l^* T_s \exp\left[i\omega_2^0 \Delta t\right]\right\} \exp\left[-\frac{\Delta t^2}{4\beta_2}\right], \quad \text{where} \quad \beta_2 = \frac{1}{\sigma_1^2} + \frac{1}{\sigma_2^2}. \tag{4}$$

T_s and T_l are the overall amplitude transmittances of the two alternative paths in the MZ interferometer. In the ideal case, when both paths are equally probable, the local visibility of the coincidence-count rate interference pattern is

$$V(\Delta t) = \exp\left[-\frac{\Delta t^2}{4\beta_2}\right]. \tag{5}$$

If we assume the geometric filtering only ($\sigma_1 = \sigma_2 = \sigma$), the visibility in MZ interferometer simplifies to a form

$$V(\Delta t) = \exp\left[-\frac{\sigma^2 \Delta t^2}{8}\right]. \tag{6}$$

Right panel of Fig. 2 shows the coincidence-count interference visibility measured with no filters (diamonds), and with narrow band interference filter centered

at 826.4 nm, FWHM =1.8 nm (squares). The dotted line is a Gaussian fit to these data. The left panel of Fig. 2 shows the corresponding spectra. FWHM of the geometric filtering is found to be 5.3 nm (dotted line). The normalized transmittance spectrum of the interference filter is shown with the solid line and the corresponding interference visibility plotted in the right panel fit well with the measured data. Narrowing of the spectrum of signal photons from 5.3 nm to 1.8 nm yields the broadening of the coincidence-count interference pattern from 160 μm to 350 μm.

2.2. Setup with A Fabry-Perot resonator (FP)

FP provides a *two-orders-of-magnitude narrower frequency filter* than the narrow band interference filter. The geometric filtering also takes place in this case.

The interference term is found to be

$$\rho(\Delta t) = \frac{2}{C_{FP}}\mathrm{Re}\left\{T_l^* T_s \sum_{n=-\infty}^{\infty} V_0^{|n|} \exp\left[i(\omega_2^0 \Delta t + n\varphi_0)\right] \exp\left[-\frac{(\Delta t - nt_0)^2}{4\beta_2}\right]\right\},$$

$$t_0 = 2\frac{l_F}{c}, \quad \text{and} \quad \varphi_0 = \omega_1^0 t_0. \tag{7}$$

t_0 determines the time of one roundtrip in the FP resonator, φ_0 is a phase factor acquired in one roundtrip. The n-th term of the sum corresponds to the case that the signal photon propagates just $|n|$ times through the FP. The n-th term contribution is peaked around the detuning value $\Delta t = nt_0$. The width of the peak is the same as in the case without the FP resonator, determined by the spectral width of the entangled photons [13]. If these peaks are *narrower* than t_0, then the visibility is a modulated function. If these peaks are *wider* than t_0, then the visibility dependence is smooth function. The upper envelope of the visibility dependence (7) is found as

$$V^{\mathrm{upper}}(\Delta t) = V_0^{\frac{|\Delta t|}{t_0}} = \left(1 + \frac{2}{\gamma}(1 - \sqrt{1+\gamma})\right)^{\frac{|\Delta t|}{t_0}}, \quad \gamma = \left(\frac{2F}{\pi}\right)^2, \tag{8}$$

where parameter F is the finesse of the FP resonator.

2.2.1. Multiple lines of the FP resonator

The transmittance spectrum of the FP resonator is a periodic function with narrow peaks at a distance given by a free spectral range. In our case, $\lambda_{FSR} = \frac{1}{2}\lambda^2/l_F \approx$ 3.6 nm. The spectrum of the signal photon is limited within the interval given by the geometric filtering (FWHM=5.3 nm). If we scan the width of the FP within one quarter of the wavelength the transmittance spectrum changes and the calculated coincidence-count interference visibility changes as well (see Fig. 3). In all cases the high-visibility region is broadened considerably according to Eq. (8), moreover the dependence is modulated with the period corresponding to one roundtrip in the FP resonator. Figure 3a) shows the first limit case, $l_F = 94.80$ μm. The spectrum is dominated by two equivalently strong maxima and the calculated visibility

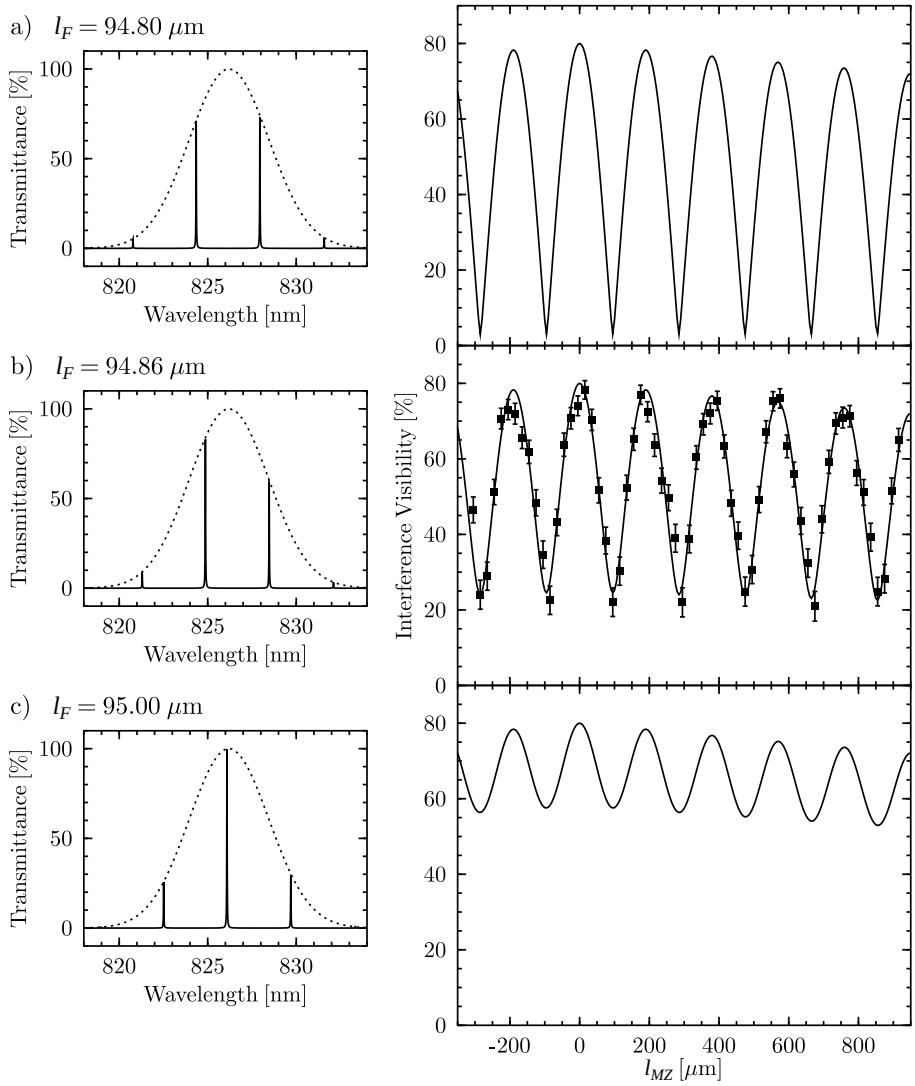

Fig. 3. Spectra of the signal photons (left panel) and the corresponding coincidence-count interference visibility as a function of the relative delay l_{MZ} (right panel); squares − measured data, lines − theory calculated with parameter $F = 150$ for three different values of l_F.

modulation is the deepest. Figure 3c) shows the other limit case, $l_F = 95.00\ \mu$m. The spectrum has one dominant peak and two smaller satellites at both sides. The visibility modulation is the smallest. Squares in the right panel of Fig. 3b) shows the measured interference visibility. The period of the visibility oscillations yields

$l_F \approx 95$ μm. Comparing the measured depth of the modulation gives more accurate l_F within one quarter of the wavelength, $l_F = 94.86$ μm.

2.2.2. Single line of the FP resonator

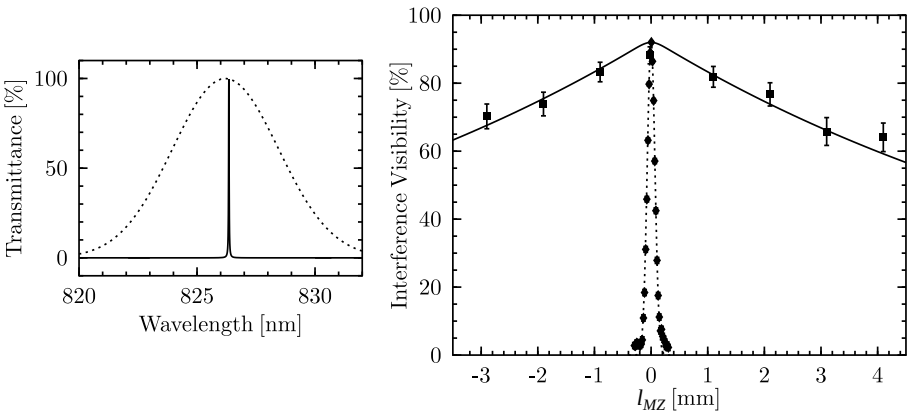

Fig. 4. Right panel: coincidence-count interference visibility as a function of the relative delay l_{MZ} measured without any filter (diamonds, same as in Fig. 2) and with both the FP resonator and the narrow band interference filter in the signal-photon path (squares). The solid line is the fit according to Eq. (7). Left panel: corresponding spectra.

We can use the FP resonator together with the narrow band interference filter in order to select just a singe line of the FP resonator. It is possible due to the fact, that the FWHM of the narrow band interference filter (1.8 nm) is narrower than the free spectral range of the FP resonator (3.6 nm). It should be stressed out, that the width of a single peak is about 0.024 nm, which is two-orders-of-magnitude narrower than the interference filter. Scanning the FP length we are able to position a single narrow transmittance peak to the center of the interference filter, $l_F = 95.03$ μm. With this setting the high-visibility region is broadened considerably and *no oscillations* of the measured visibility appear. The theoretical dependence of the interference visibility is also given by Eq. (8).

3. Time correlations

Our fiber implementation of the HOM interferometric setup is drawn in Fig. 5. The normalized coincidence-count rate R_n^{HOM} as a function of relative delay between the signal and idler photons is

$$R_n^{HOM}(\Delta t) = 1 - \rho^{HOM}(\Delta t). \tag{9}$$

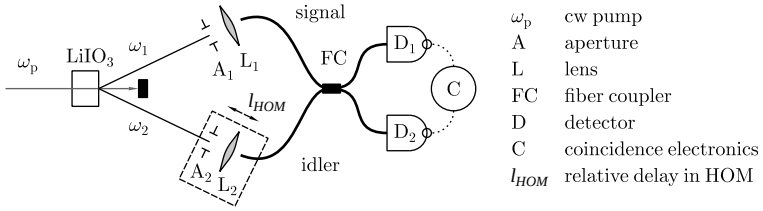

Fig. 5. Experimental setup for the Hong-Ou-Mandel interference measurement.

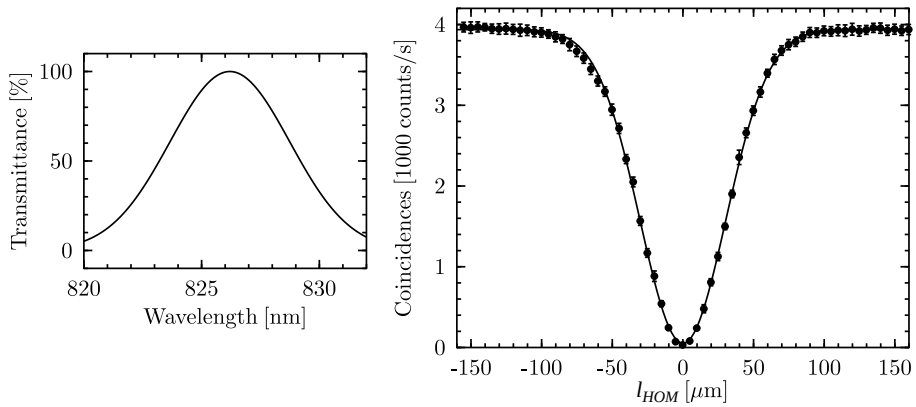

Fig. 6. Right panel: coincidence-counts in the Hong-Ou-Mandel interferometer as a function of the path difference of the interferometer's arms l_{HOM}: measured data (dots) and theoretical fit (solid line). Left panel: corresponding spectrum.

Assuming the geometric filtering only ($\sigma_1 = \sigma_2 = \sigma$), the interference term for HOM interferometer reads

$$\rho^{HOM}(\Delta t) = \exp\left[-\frac{\sigma^2 \Delta t^2}{2}\right]. \tag{10}$$

We can compare the theoretical width of the HOM dip given by Eq. (10) with the width of the interference visibility peak measured with MZ interferometer, as described by Eq. (6). Theoretically the HOM dip should be half wide compared with the width of the interference peak measured under the same conditions with the MZ interferometer. Gaussian fit to the measured dip shown in the right panel of Fig. 6 yields the spectrum of the geometric filtering, FWHM=6.0 nm. This spectral width is slightly larger than the one obtained with the MZ interferometer (5.3 nm). This small difference is probably due to the slight readjustment needed after rebuilding the setup (compare Figs. 1 and 5).

4. Conclusions

The second- and fourth-order interference experiments testing the two-photon fields generated in spontaneous parametric down-conversion were performed and explained.

We placed the narrow frequency filter in the signal beam and observed an effective prolongation of the coherence length (in the MZ interferometer placed in the idler-beam path) and a substantial increase of visibility in a coincidence-count measurement. This prolongation is the consequence of *the correlation of energies* of the two beams given by the two-photon state Eq. (1). This individual experimental result can be explained also classically, i.e. it could be achieved also with a certain separable state of two photons.

We measured also the HOM-interference dip with the same photon source to confirm that the signal and idler photons comprising one pair are also *correlated in time*. This individual experimental result can again be explained classically. However, no classical description of both experiments (energy/time) can be developed. I.e., only the entangled two-photon state can exhibit both these correlations together.

Acknowledgment(s)

This research was supported by the Ministry of Education of the Czech Republic under grants LN00A015, CEZ J14/98, RN19982003012, and by EU grant under QIPC project IST-1999-13071 (QUICOV).

References

1. C.K. Hong, L. Mandel, *Phys. Rev. A* **31**, (1985) 2409.
2. J. Peřina, Z. Hradil, and B. Jurčo: *"Quantum Optics and Fundamentals of Physics"*, Kluwer, Dordrecht, 1994.
3. M.H. Rubin, *Phys. Rev. A* **54**, (1996) 5349.
4. J.D. Franson, *Phys. Rev. Lett.* **62**, (1989) 2205.
5. J.D. Franson, *Phys. Rev. Lett.* **67**, (1991) 290.
6. J.G. Rarity, P.R. Tapster, *Phys. Rev. A* **45**, (1992) 2052.
7. P.G. Kwiat, A.M. Steinberg, R.Y. Chiao, *Phys. Rev. A* **47**, (1993) R2472.
8. P.G. Kwiat, R. Y. Chiao, *Phys. Rev. Lett.* **66**, (1991) 588.
9. M. Dušek, *Czech. J. Phys.* **46**, (1996) 921.
10. P. Trojek, J. Peřina, Jr., *Czech. J. Phys.* **53**, (2003) 335.
11. J. Soubusta, J. Peřina Jr., M. Hendrych, O. Haderka, P. Trojek, M. Dušek, *Phys. Lett. A* **319**, (2003) 251; arXiv quant-ph/0306020.
12. C.K. Hong, Z.Y. Ou, L. Mandel, *Phys. Rev. Lett.* **59**, (1987) 2044.
13. J. Peřina. Jr., *Opt. Commun.* **221**, (2003) 153.